Heterocyclic Letters
Vol. 16| No.1|129-138|Nov-Jan|2026
ISSN : (print) 2231–3087 / (online) 2230-9632
CODEN: HLEEAI
http://heteroletters.org

HETEROCYCLIC ALKALOID MEDIATED GREEN SYNTHESIS OF SELENIUM NANOPARTICLES FROM *Berberis aristata* AND THEIR ANTIBACTERIAL ACTIVITY

Vivek Jedhe[a]*, Suraj Adole[b], Pallavi Pantawane[c], Sanjiv Patil[d] and Bhuvaneshwari Mehere[e]

[a,b,c,e]*Department of Biochemistry, Dr. Ambedkar College, Dikshabhoomi, Nagpur, Maharashtra, India*
[d]*Department of Biochemistry, Shri Shivaji College of Arts, Commerce and Science, Akola, Maharashtra, India*
**Corresponding Author Email: vivekbiochem@gmail.com*

ABSTRACT:
The present study reports the heterocyclic alkaloid mediated green synthesis of selenium nanoparticles (SeNPs) using aqueous root extract of *Berberis aristata* (BASeNP). The plant rich in isoquinoline type heterocyclic alkaloids such as berberine and palmatine. These heterocycles act as natural reductants and stabilizing ligands during nanoparticle formation. The successful synthesis was confirmed by characteristic surface plasmon resonance band at 280–290 nm. FTIR spectra revealed distinct functional vibrations corresponding to –OH, N–H, C=O, and aromatic heterocyclic alkaloids, with noticeable shifts after nanoparticle formation, indicating their involvement in reduction and capping. XRD analysis displayed sharp diffraction peaks consistent with crystalline elemental selenium, while TEM and SEM studies confirmed predominantly spherical nanoparticles ranging from 10 nm to 40 nm with good colloidal stability. The antimicrobial efficacy of BASeNPs was evaluated against *Staphylococcus aureus* and *Escherichia coli* using agar well diffusion and broth microdilution methods. BASeNPs exhibited dose-dependent antibacterial activity, showing greater inhibition against *S. aureus*. These findings establish *B. aristata* heterocyclic alkaloids as efficient biogenic agents for eco-friendly SeNP synthesis and highlight the potential of BASeNPs as effective antimicrobial nanomaterials.

KEY WORDS: *Berberis aristata*, heterocyclic alkaloids, green synthesis, selenium nanoparticles, antimicrobial activity.

1 INTRODUCTION

The increasing prevalence of antimicrobial resistance has intensified the search for novel, effective and biocompatible therapeutic agents. In the past few years, green nanobiotechnology has materialised as a favourable tactic for the environment friendly synthesis of metalloid and metallic nanoparticles using phyto-derived natural chemicals. These plant-derived

phytochemicals act as reducing as well as stabilizing agents. Comparing all the selenium nanoparticles have gain considerable tension due to their bio compatibility reduced the toxicity potent antioxidant activity and broad spectrum antimicrobial properties as compared to inorganic selenium form. The use of medicinal plant extract for nanoparticle green synthesis approach gives additional advantage by incorporating bioactive phytochemicals into the nanoparticles surface. This results in synergistic enhancement in their biological effects. Indian Barberry (Berberis aristata DC) commonly known as 'Daru Haridra'[i] is a traditionally known medicinal plant for its use in ayurvedic formulations. Its roots are particularly rich in isoquinoline heterocyclic alkaloids, such as berberine, palmatine, and jatrorrhizine[ii], which possess strong reducing abilities and play a crucial role in nanoparticle formation. These heterocyclic alkaloids also confer significant antimicrobial, anti-inflammatory, immunomodulatory and hepatoprotective properties to the plant, making it an ideal candidate for green biosynthesis of functional nanoparticles. Considering the phytochemical richness of *B. aristata* and the biomedical importance of selenium nanoparticles, the present study aims to investigate the heterocyclic alkaloid mediated green synthesis of selenium nanoparticles using *B. aristata* root aqueous extract, their physiochemical characterization and the evaluation of their antimicrobial potential. This work will highlights the value of *B. aristata* as a potent biogenic source for developing suitable, plant mediated, and cost effective, non toxic but promising antimicrobial applications

2 MATERIALS AND METHODS:

2.1 Herbal Material and Specimen Authentication

Dried roots of *Berberis aristata* were procured from a certified local herbal vendor in Maharashtra, India. Plant identification and authentication were performed by senior taxonomists from the Department of Botany, Rashtrasant Tukadoji Maharaj Nagpur University. A voucher specimen was prepared and deposited in the Department of Biochemistry, Dr. Ambedkar College, Dikshabhoomi, Nagpur (Ref. No.: A.C./B.C./2/2022–23). The roots were washed thoroughly with sterile distilled water, light avoiding dried at a comfortable temperature of room, and ground down using a laboratory grinder[iii] . The powdered material was stored in airtight containers until extraction.

2.2 Preparation of Aqueous Root Extract

50 gm of B. aristata root powder crushed was mixed with 500 ml of double distilled water in 1 L beaker. The mixture heated at 60±2°C for 1 hour with stirring on thermostatic waterbath (BIO TECHNICS, India). The extract was cooled to room temperature, filtered through Whatman No. 1(HiMedia, India) filter paper[iv], and postfiltered by centrifugation at speeds 9500 rpm to 1000 rpm for 5±2 minutes to filter coarse particles. The final clear extract was refrigerated for downstream use at 4°C.

2.3 Phytochemical Screening Aqueous Root Extract

2.3.1 Qualitative Content Analysis

Standard colorimetric and precipitation tests were performed to detect major classes of phytochemicals including alkaloids, saponins, glycosides, reducing sugars, phytosterols, flavonoids, and terpenoids. Dragendorff's test indicated strong alkaloid presence, while Fehling's, Salkowski, Liebermann–Burchard, and ferric chloride assays confirmed the presence of reducing sugars, phytosterols, terpenoids, and phenolic compounds, respectively[v].

2.3.2 Quantitative HPTLC Profiling

High-Performance Thin Layer Chromatography (HPTLC)[ii] was conducted using silica gel 60 F254 plates. Quercetin and berberine hydrochloride standards were applied using a CAMAG ATS applicator. Two mobile phases were used: for Flavonoid analysis: toluene:ethyl acetate: methanol (4:10:2.5) and for Alkaloid profiling: butanol:glacial acetic acid:water (70:10:20).

Plates were dried and scanned at 254 and 366 nm using a CAMAG TLC Scanner. Peak areas were compared with standards, confirming significant amounts of berberine and quercetin in the extract.

2.4 Green Synthesis of Selenium Nanoparticles (BASeNPs)

Selenium nanoparticles were synthesized using sodium selenite (Na_2SeO_3, 10 mM) as the precursor. Ten millilitres of Na_2SeO_3 solution were stirred while adding 2–10 mL of *B. aristata* root extract dropwise. The most stable and promising synthesis observed with 4ml extract. The reaction mixture was maintained at 37^0C in dark condition for 24 hrs with gentle stirring on magnetic stirrer with 150rpm. A distinct color change from yellow to brick red indicated the successful reduction of selenite into elemental selenium. Progress of synthesis monitored using UV–Visible spectrophotometer (Shimadzu UV-1900i) between 200–400 nm. The nanoparticles were collected by centrifugation at 15,000 × g for 30 minutes [vi], washed with distilled water and ethanol. After dried overnight and ground into fine powder mechanically with mortar and piston, powder stored at 4°C.

2.5 Characterization of BASeNPs

After synthesizing brick red color BASeNPs, the structural characterization performed using a suite of advanced analytical techniques:

2.5.1 UV–Visible Spectroscopy

UV–Visible spectroscopy recorded the absorbance profile of the SeNPs between 200 nm – 600 nm. The results of distinct Surface Plasmon Resonance (SPR) peaks, for confirmation of successful nanoparticle formation, were compared with earlier literature[vii].

2.5.2 Fourier Transform Infrared Spectroscopy (FTIR)

FTIR spectra (400–4000 cm^{-1}) were recorded using a Thermo Nicolet Avatar 370 spectrophotometer to identify functional groups[viii] responsible for reduction and capping. Peaks indicated O–H, N–H, C=O, C–O, and Se–O/Se–Se vibrations, confirming phytochemical–nanoparticle interactions.

2.5.3 X-Ray Diffraction (XRD)

Crystallinity and phase purity were evaluated using a Bruker AXS D8 Advance diffractometer[ix] with CuKα radiation (λ = 1.5405 Å). Diffraction peaks matched elemental selenium, and crystallite size was calculated using the Scherrer equation[x].

2.5.4 Scanning Electron Microscopy (SEM) and Transmission Electron Microscopy (TEM)

SEM (JEOL JEM-6390LV) examined surface morphology, while HRTEM (JEOL JEM-2100) confirmed spherical/oval particles sized [xi]. All imaging was performed at STIC, Cochin, Kerala

2.6 Antimicrobial Activity Evaluation

2.6.1 Bacterial Strains

Standard strains of *Staphylococcus aureus* (ATCC 25923) and *Escherichia coli* (ATCC 25922) were used. Cultures were grown in Mueller–Hinton Broth (MHB) and standardized to a 0.5 McFarland turbidity (≈1.5×10^8 CFU/mL) before use[xii].

2.6.2 Agar Well Diffusion Assay

Mueller–Hinton Agar (MHA) plates were swabbed with bacterial inoculum. Wells (6 mm diameter) were filled with BASeNP suspensions (25, 50, 100 µg/mL). Plates were incubated at 37°C for 18–24 hours, and zones of inhibition measured. Ciprofloxacin served as a positive control, and sterile water as negative control [xiii].

2.6.3 Minimum Inhibitory Concentration (MIC)

MIC was determined using the broth microdilution method[xiv] in 96-well plates with nanoparticle concentrations of 25–100 µg/mL. Wells were inoculated with 10^6 CFU/mL and incubated at 37°C for 24 hours. Growth was assessed visually or by measuring OD600 using a Robonik Readwell Touch microplate reader. MIC was recorded as the lowest concentration showing no visible growth.

3 RESULTS AND DISCUSSION

Because of the presence of diverse bioactive secondary metabolites having therapeutic values, plants continue to draw considerable interest from scientific and pharmaceutical communities. Many of these metabolites act as strong antioxidants and exhibit notable antimicrobial and anticancer activities. These properties offer an eco-friendly, nutritionally rich, and therapeutically valuable source of metabolites that act as strong antioxidants and exhibit notable antimicrobial and anticancer activities. Plant compounds such as heterocyclic constituents were recognized as effective reducing and stabilizing agents in the green synthesis of biologically active nanoparticles. *Berberis aristata* is especially distinguished for its high content of heterocyclic alkaloids like berberine, along with flavonoids and phenolic compounds, which contribute both to its pharmacological relevance and its capacity to support nanoparticle synthesis. Despite the extensive medicinal use of *B. aristata*, its application as a biogenic source for constructing selenium nanoparticles has been relatively underexplored. The present findings show that the heterocyclic alkaloid rich root extract of *B. aristata* efficiently facilitates the formation of stable, biofunctionalized selenium nanoparticles, highlighting its promising role in green nanotechnology.

3.1 Phytochemical Composition of Berberis aristata Root Extract

Qualitative screening of the aqueous *B. aristata* root extract confirmed the presence of major bioactive groups, including alkaloids, flavonoids, saponins, glycosides, reducing sugars, phytosterols, and terpenoids, whereas proteins and tannins were absent. The strong Dragendorff's reaction confirmed the presence of abundant isoquinoline alkaloids such as berberine, palmatine, and jatrorrhizine. Which may act as potent electron donors and reducing agents, and as a capping agent for nanoparticles. Also, it plays a key role in converting selenite ions into elemental selenium. The phytochemical composition of the extract is shown in Table 1 below.

Table 1. Qualitative Phytochemical Screening of *Berberis aristata* Root Extract

Phytochemical Group	Test Performed	Observation	Presence
Alkaloids	Dragendorff's test	Orange precipitate	+++
Flavonoids	Ferric chloride test	Greenish-black coloration	++
Reducing sugars	Fehling's test	Brick-red precipitate	++
Glycosides	Liebermann–Burchard test	Brown ring formation	+
Saponins	Froth test	Persistent foam	+
Phytosterols	Salkowski test	Reddish-brown layer	+
Terpenoids	Liebermann–Burchard test	Green coloration	+
Phenolics	Ferric chloride test	Dark blue color	++
Proteins	Biuret test	No violet color	–
Tannins	Lead acetate test	No precipitate	–

+++ = Strongly present, ++ = Moderately present, + = Trace amounts, – = Absent

HPTLC profile validated the phytochemical richness of the green synthesised extract. Table 2 provides the HPTLC profile of the root extract, highlighting characteristic Rf values and peak areas that confirm the abundance of isoquinoline alkaloids and flavonoids. Distinct and well-resolved bands corresponding to quercetin ($Rf \approx 0.72$) and berberine ($Rf \approx 0.47$) were observed. This confirming the presence of flavonoids and heterocyclic alkaloids in significant quantities. Overall, the phytochemical analysis of the root extract provides the chromatographic fingerprint of a complex mixture of secondary metabolites which may capable of reducing, stabilizing, and capping selenium nanoparticles during biosynthesis.

Table 2. HPTLC Profiling of Major Phytochemicals in *B. aristata* Extract

Compound	Rf Value	Detection (nm)	Wavelength	Peak Area (%)	Interpretation
Berberine	0.47	366 nm		High	Major alkaloid present
Palmatine	0.52	366 nm		Moderate	Isoquinoline alkaloid
Jatrorrhizine	0.39	366 nm		Low	Minor alkaloid
Quercetin	0.72	254 nm		Moderate	Major flavonoid present
Other flavonoids	0.60–0.80	254 nm		Low–Moderate	Mixed phenolics

3.2 Structural Characterization of BASeNPs

3.2.1 Visual Confirmation and UV–Visible Spectroscopy of BASeNPs

The successful synthesis of BASeNPs was first indicated by visible color change from pale yellow to brick red color. The material shows characteristic Surface Plasmon Resonance (SPR) peak at ~290 nm in UV visible spectrophotometer consistent with the plant-mediated selenium nanoparticles reported in the literature. As shown in figure 1 a, the The absorption profile (200–800 nm) showed a strong, sharp band characteristic of stable SeNP formation, confirming effective phytochemical-mediated reduction and nucleation.

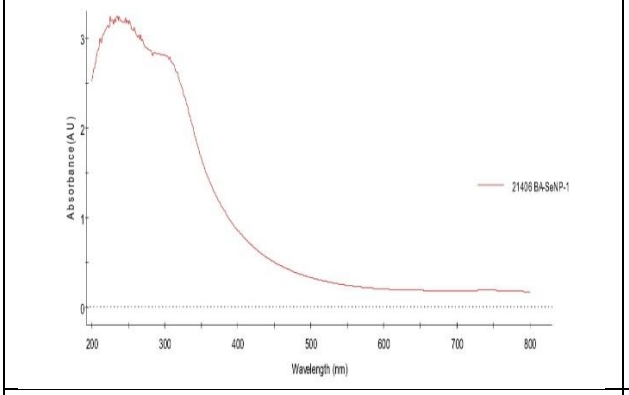

Figure 1 a. UV–Visible Absorption Spectrum of BASeNPs

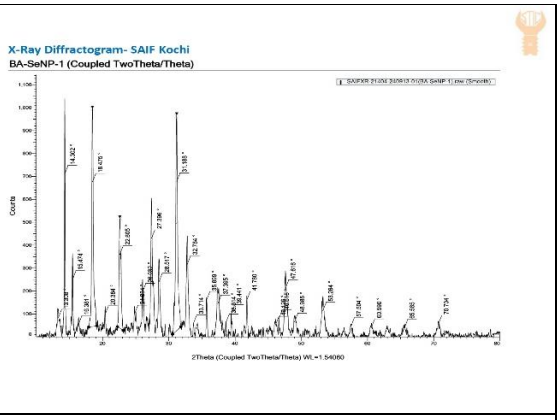

Figure 1 b. XRD Diffraction Pattern of BASeNPs

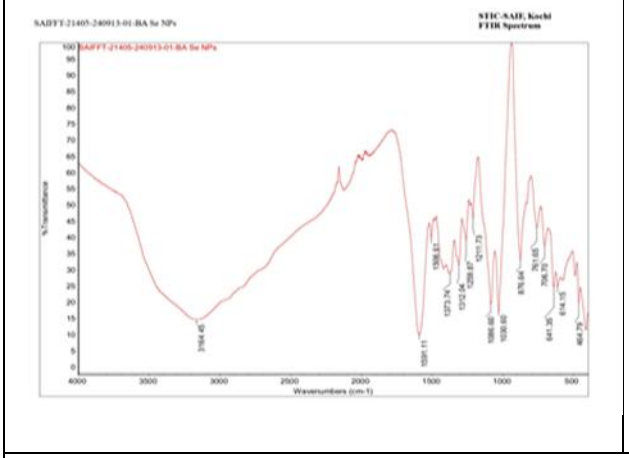

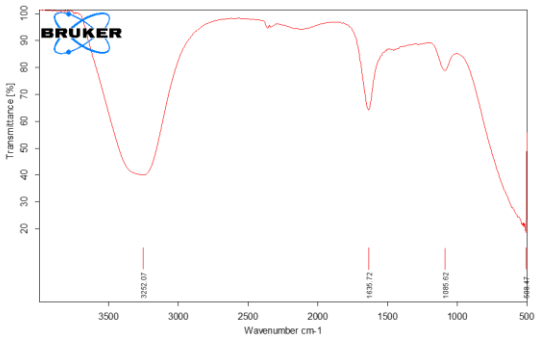

Figure 1 c. FTIR Spectrum of BASeNPs and B. aristata Root Extract:

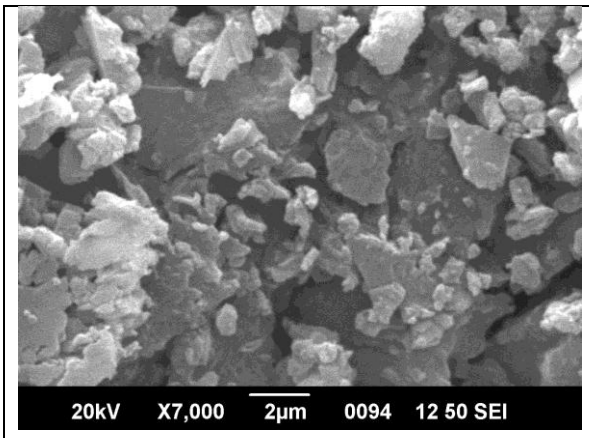

***Figure 1 d*. SEM Micrograph of BASeNPs**

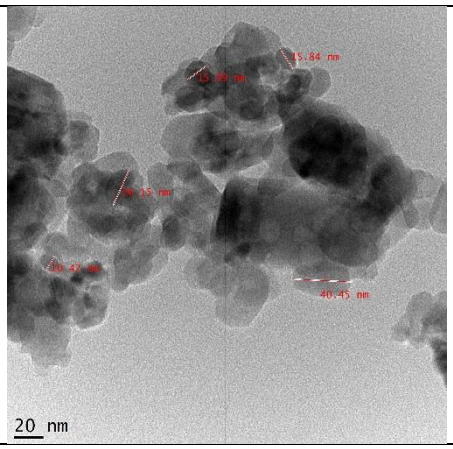

***Figure 1 e*. TEM Image and Particle Size Distribution of BASeNPs:**

3.2.2 XRD Analysis: Crystallinity of BASeNPs

As shown in Figure 1 b: XRD patterns of BASeNPs displayed sharp and intense peaks at 2θ values including 14.32°, 18.47°, 22.60°, 27.36°, 31.18°, and 32.72°, corresponding to crystalline planes of elemental selenium. The absence of amorphous or impurity peaks confirmed high purity of the biosynthesized nanoparticles. The averaged crystalline size was calculated using the Scherrer equation, was reported ~14 nm, matching with the dimensions observed in TEM. These results affirm that the *B. aristata* phytochemicals produced well defined nanocrystalline selenium with excellent structural uniformity. The XRD data and corresponding crystallite sizes are provided in Table 3.

Table 3. XRD Peak Assignments and Crystallite Size of BASeNPs

2θ (Degrees)	Miller Indices (hkl)	Peak Intensity	Crystallite Size (nm)	Reference Standard
14.32	(100)	Medium	13.5	Hexagonal Se
18.47	(101)	Medium	14.2	Hexagonal Se
22.60	(110)	Strong	14.0	Hexagonal Se
27.36	(111)	Strong	14.5	Hexagonal Se
31.18	(201)	Weak	13.8	Hexagonal Se
32.72	(202)	Medium	14.1	Hexagonal Se

3.2.3 FTIR Analysis: Functional Group Interactions

As, shown in figure 1c, the FTIR spectra of BASeNPs showed multiple absorption peaks representing the functional groups involved in reduction and stabilization. Prominent bands included O–H stretching (~3164 cm^{-1}), C–H stretching (~2900 cm^{-1}), amide and carbonyl peaks between 1600–1700 cm^{-1}, and C–O/C–N vibrations in the 1000–1300 cm^{-1} region. Peaks at lower wavenumbers (<700 cm^{-1}) indicated Se–O and Se–Se bond formation. The FTIR results shown here confirmed successful capping by phytochemicals from *B. aristata*, contributing to nanoparticle stability and bioactivity. Table 4 summarizes the FTIR peak assignments of the extract and BASeNPs, highlighting the functional group shifts involved in the reduction and stabilization of selenium nanoparticles.

Table 4. FTIR Peak Assignments for Extract and BASeNPs

Wavenumber (cm^{-1})	Functional Group Assigned	Extract	BASeNPs	Role in Synthesis
3164	O–H stretching	Strong	Shifted	Reduction & capping
2900	C–H stretching	Moderate	Shifted	Stabilization
1700–1600	C=O, amide I	Sharp	Shifted	Binding to SeNP surface
1400–1500	Aromatic C=C	Present	Slight shift	Alkaloid involvement
1000–1300	C–O / C–N	Strong	Strong	Surface functionalization
<700	Se–O, Se–Se	Absent	Present	Nanoparticle formation indicator

3.2.4 SEM and TEM Analysis: Morphology and Size Distribution

As shown in Figure 1 d, the SEM micrographs revealed aggregated clusters of BASeNPs with rough and irregular surfaces may be due to strong intermolecular interactions and dense phytochemical capping. Figure 1 e, The TEM images provided clearer insights. The nanoparticle has with sizes ranging from 10 nm to 40 nm. The well-defined boundaries of spherical and oval intense crystalline cores in the TEM images supported the XRD findings. These observations confirm successful biosynthesis and indicate that plant functionalised capping agents effectively stabilized the nanoparticles, reducing agglomeration

3.3 Antimicrobial Activity of BASeNPs

3.3.1 Agar Well Diffusion Assay

Table 5 summarizes the antibacterial activity of BASeNPs, showing a concentration-dependent increase in the zone of inhibition against both S. aureus and E. coli. In the present work, the antibacterial activity of the selenium nanoparticles synthesized from *Berberis aristata* root extract (BASeNPs) was examined through the agar well diffusion assay.

Table 5. Antibacterial Activity (Zone of Inhibition) of BASeNPs

Concentration (µg/mL)	S. aureus (mm)	E. coli (mm)	Positive Control (Ciprofloxacin)
25	11 ± 0.5	8 ± 0.4	29 ± 0.6
50	16 ± 0.6	12 ± 0.5	30 ± 0.5
100	21 ± 0.7	16 ± 0.5	31 ± 0.4

The results showed a clear increase in inhibition with increasing nanoparticle concentration, although the pattern differed slightly between the two bacterial strains. At 25 µg/mL, the inhibition zone against *E. coli* was comparatively small (around 8 mm), while *S. aureus* showed a slightly larger zone of about 11 mm. As the concentration increased to 50 and 100 µg/mL, the zones widened noticeably, reaching 16 mm for *E. coli* and as much as 21 mm for *S. aureus* at the highest concentration tested.

The observation shown that *S. aureus* consistently showed larger zones of inhibition than *E. coli*. This may be due to the Gram-positive bacteria lack the outer membrane layer that usually acts as a protective barrier in Gram-negative organisms. During plate observation it was observed that, the *S. aureus* zones also appeared sharper and more clearly demarcated compared to those of *E. coli*, which suggests stronger nanoparticle interaction with the Gram-positive cell surface. Overall, the report matches with earlier reports on metal and metalloid nanoparticles, where membrane damage and oxidative stress were considered the main mechanisms behind microbial inhibition. In present study the standard antibiotics ciprofloxacin produced much larger zones than BASeNPs, still BASeNPs displayed meaningful antibacterial

action, particularly at higher concentrations. This suggests that BASeNPs may have potential as supportive or alternative agents, especially for infections mediated by Gram positive pathogens.

3.3.2 MIC Determination

Table 6. MIC Values of BASeNPs Against Test Microorganisms

Organism	**MIC (µg/mL)**	**Interpretation**
Staphylococcus aureus	8	Highly sensitive
Escherichia coli	64	Moderately sensitive

When the inhibitory activities of BASeNPs was examined through MIC assay, the results followed the same general trends observed in the well diffusion assay. The MIC values for both test organisms are shown in Table 6. *S aureus* required lowest concentration of BASeNPs for visible growth inhibition.The MIC for *S. aureus* was found to be 8 µg/mL, whereas *E. coli* needed a much higher concentration of 64 µg/mL before growth was completely suppressed. This clear difference between two organisms was also noticlable during incubation. the wells containing lower concentrations for *S. aureus* remained visibly clearer compared to those inoculated with *E. coli*. The sensitivity of *S. aureus* may be due to its simple cell envelope. Since Gram-positive bacteria do not possess the outer membrane characteristic of Gram-negative species, nanoparticles may reach the peptidoglycan layer more easily. Leads to faster interaction with the membrane and intracellular components. Opposite to that, the outer lipopolysaccharide barrier of *E. coli* may have limited the direct contact between BASeNPs and the cell surface, which could explain the higher MIC value.

Another point is that the BASeNPs maintained their inhibitory effect without any noticeable clumping or precipitation during the assay. This is the indicator of reasonably good stability of the suspension throughout the incubation period. The wells at higher concentrations also appeared less turbid, supporting the possibility that BASeNPs interfere with essential metabolic processes, possibly through oxidative stress or enzyme inhibition which have been recorded for other selenium based nanomaterials.

Although ciprofloxacin exhibited a far lower MIC, the behaviour of BASeNPs is still promising. As considering that these nanoparticles were synthesized through a simple plant based route without the use of harsh chemicals. The comparatively strong response of *S. aureus* indicates that BASeNPs might be more useful in formulations targeting Gram-positive infections. However, the reduced susceptibility of *E. coli* also highlights the need for further study by optimization of particle size or surface modification or possible combination approaches with existing antibiotics.

Overall, the MIC results showed that BASeNPs have meaningful antibacterial potential. Also shows strong effect on Gram positive bacteria. BASeNPs may serve as a useful foundation for developing alternative antimicrobial strategies.

3.3.3 Overall Interpretation

The findings suggest that the root extract of *Berberis aristata* functions as an effective natural reducing and stabilizing agent in the green synthesis of selenium nanoparticles. Its rich phytochemical composition particularly the presence of alkaloids such as berberine appears to play a central role in shaping nanoparticle formation. The stable and strong antimicrobial performance of BASeNPs produced crystalline, well within the nanoscale range and coated with bioactive functional groups derived from the extract. These structural and chemical features are consistent with BASeNPs show notable antibacterial activity, indicating that BASeNPs hold considerable promise for use in antimicrobial formulations.

4 CONCLUSION

The present work shows that the root extract of *Berberis aristata* is naturally rich in heterocyclic alkaloids. These alkaloids act as both reducing and stabilizing agents in the green synthesis of selenium nanoparticles (BASeNPs). . The mixture of isoquinoline alkaloids, flavonoids, and phenolic compounds in the extract appears to support the rapid reduction of selenite ions, leading to the formation of stable nanoparticles confirmed by UV–Vis, FTIR, XRD, SEM, and TEM analyses, the nanoparticles were biofunctionalized, crystalline, and largely spherical (size 10nm to 40 nm) showed clear inhibitory activity against both *Staphylococcus aureus* and *Escherichia coli*. It showed that the inhibiton increased with concentration in both the diffusion and MIC assays. The stronger effect shown on *S. aureus* due to the known structural differences between Gram-positive and Gram-negative bacteria. The findings suggest that the nanoparticles interact more readily with the Gram-positive cell wall. Taken together, these observations suggest that *Berberis aristata* is a promising botanical source for producing biogenic selenium nanoparticles and that the resulting BASeNPs may have valuable applications in antimicrobial product development and broader areas of nanobiotechnology.

5 ACKNOWLEDGEMENT

The authors express their sincere appreciation to the Department of Biochemistry, Dr. Ambedkar College, Nagpur for providing the laboratory facilities and overall research support. Dr. Dongarwar and Dr. Jadhao from RTM Nagpur University for identifying the plant. We also acknowledge the Department of Biochemistry from Shri Shivaji College, Akola for their help during antimicrobial studies. FTIR, XRD, SEM, and TEM facilities through the Central Instrumentation Facility, Kochin is gratefully recognized.

6. REFERENCES

i. Choudhary S.; Kaurav H.; Madhusudan S.; Chaudhary G.; Daruharidra (Berberis aristata): review based upon its ayurvedic properties; *Int. J. Res. Appl. Sci. Biotechnol.*; 2021, **8**(2), 98–106.

ii. Marchelak A.; Gieleta M.; Krasocka W.; Magiera A.; Berberis aristata DC. (Indian barberry): current insight into botanical, phytochemical, and pharmacological aspects, pharmacokinetics, safety of use, and modern therapeutic applications; *Fitoterapia*; 2025, **106539**.

iii. Kshirsagar P. R.; Pai S. R.; Nimbalkar M. S.; Gaikwad N. B.; Quantitative determination of three pentacyclic triterpenes from five *Swertia* L. species endemic to Western Ghats, India, using RP-HPLC analysis; *Nat. Prod. Res.*; 2015, **29**(19), 1783–1788.

iv. Olugbemi T. I.; Green synthesis of silver nanoparticles from aqueous extract of unripe pawpaw peel and its antimicrobial and antioxidant property; *FEPI-JOPAS*; 2019, **1**(1), 203–209.

v. Goswami R.; Arora N.; Ambwani S.; Singh J. L.; Mrigesh M.; Bhat A. A.; Maansi; Manzoor I.; Phytochemical, antioxidant and proximate analysis of *Berberis aristata* roots; *Int. J. Adv. Biochem. Res.*; 2024, **8**(8, Suppl.), 608–615.

vi. Markelonis A. R.; Wang J. S.; Ullrich B.; Wai C. M.; Brown G. J.; Nanoparticle film deposition using a simple and fast centrifuge sedimentation method; *Appl. Nanosci.*; 2015, **5**(4), 457–468.

vii. Ahamad Tarmizi A. A.; Nik Ramli N. N.; Adam S. H.; Abdul Mutalib M.; Mokhtar M. H.; Tang S. G. H.; Phytofabrication of selenium nanoparticles with *Moringa oleifera* (MO-SeNPs) and exploring its antioxidant and antidiabetic potential; *Molecules*; 2023, **28**(14), 5322.

viii. Pasieczna-Patkowska S.; Cichy M.; Flieger J.; Application of Fourier transform infrared (FTIR) spectroscopy in characterization of green synthesized nanoparticles; *Molecules*; 2025, **30**(3), 684.

ix. Akbari B.; Tavandashti M. P.; Zandrahimi M.; Particle size characterization of nanoparticles – a practical approach; *Iran. J. Mater. Sci. Eng.*; 2011, **8**(2), 48–56.

x. Zhao Y. H.; Zhang K.; Lu K.; Structure characteristics of nanocrystalline element selenium with different grain sizes; *Phys. Rev. B*; 1997, **56**(22), 14322.

xi. Talam S.; Karumuri S. R.; Gunnam N.; Synthesis, characterization, and spectroscopic properties of ZnO nanoparticles; *Int. Scholarly Res. Notices*; 2012, **2012**, 372505.

xii. Altuner E. M.; Inoculum standardisation: ensuring reliable antimicrobial study outcomes; *altuner.me*; 2025, **5**(29), 1–5.

xiii. Nawaz A.; Ali S. M.; Rana N. F.; Tanweer T.; Batool A.; Webster T. J.; Iqbal A.; Ciprofloxacin-loaded gold nanoparticles against antimicrobial resistance: an *in vivo* assessment; *Nanomaterials*; 2021, **11**(11), 3152.

xiv. Radhakrishnan V. S.; Reddy Mudiam M. K.; Kumar M.; Dwivedi S. P.; Singh S. P.; Prasad T.; Silver nanoparticles induced alterations in multiple cellular targets, which are critical for drug susceptibilities and pathogenicity in fungal pathogen (*Candida albicans*); *Int. J. Nanomed.*; 2018, **13**, 2647–2663.

Received on December 6, 2025.